Nonlinear Dynamics of MEMS Arches Under Harmonic Electrostatic Actuation

Mohammad I. Younis, *Member, ASME*, Hassen M. Ouakad, *Student Member, ASME*, Fadi M. Alsaleem, *Student Member, ASME*, Ronald Miles, *Member, ASME*, and Weili Cui, *Member, ASME*

***Abstract*—We present an investigation of the nonlinear dynamics of clamped–clamped micromachined arches when actuated by a dc electrostatic load superimposed on an ac harmonic load. The Galerkin method is used to discretize the distributed-parameter model of a shallow arch to obtain a reduced-order model. The static response of the arch due to a dc load actuation is simulated, and the results are validated by comparing them to experimental data. The dynamic response of the arch to a combined dc load and ac harmonic load is studied when excited near its fundamental natural frequency, twice its fundamental natural frequency, and near other higher harmonic modes. The results show a variety of interesting nonlinear phenomena, such as hysteresis, softening behavior, dynamic snap-through, and dynamic pull-in. The results are also shown demonstrating the potential to use microelectromechanical systems (MEMS) arches as bandpass filters and low-powered switches. An experimental work is conducted to test arches realized of curved polysilicon microbeams when excited by dc and ac loads. Experimental data are shown for the softening behavior and the dynamic pull-in of the curved microbeams. [2009-0180]**

***Index Terms*—Arches, dynamic pull-in, dynamic snap-through, electrostatic actuation, microelectromechanical systems (MEMS).**

I. Introduction

MICROMACHINED shallow arches have been under increasing focus in recent years in the microelectromechanical systems (MEMS) community because of their unique attractive features. One major advantage is their bistability nature, which makes them suitable for switching and actuation applications. In particular, bistable structures, such as arches and buckled beams, do not require power to hold them down in either stable states (the on or off positions as switches); they need power only during transition between the two states. Another advantage in actuation applications is that they can be displaced in large strokes compared to straight and monostable structures. Both arches and buckled structures share the bistability advantages, and hence, both have been investigated extensively in the MEMS literature. However, arches have the advantage of not requiring permanent axial force or stress to be actuated, which is usually hard to be controlled through microfabrication. In addition, because the curvature of arches is predetermined from fabrication, their response (the stroke) is more predictable and controllable compared to buckled beams. Qui *et al.* were among the first who recognized these advantages [1]. They have fabricated a stress-free curved beam, realized from two beams connected in the middle, for easier and more controllable snap-through motion.

Curved clamped–clamped microbeams, arches or buckled beams, have been the mostly used bistable structures for a variety of MEMS actuation applications. For example, curved microbeams have been used as acceleration-threshold switches [2], an artificial muscle actuator [3], to deliver electrical pulses in the human body [4], and as a mechanical memory for data storage [5]. Most of the literature has been focused on utilizing the structural instability snap-through in clamped–clamped arches and buckled microbeams as a static phenomenon due to the actuation of static forces. Those forces can be mechanical [1], magnetic [6]–[8], thermal [9], [10], comb-drive electrostatic [4], [11]–[13], and parallel-plate capacitive [2], [14]–[18].

When actuating a curved beam by a parallel-plate electrostatic force, its stability problem becomes very interesting. Previous works have shown that curved microbeams may exhibit snap-through or pull-in instability, depending on the interaction between mechanical and electrostatic forces [13]–[18]. Zhang *et al.* [14] and Krylov *et al.* [15] conducted theoretical and experimental investigations on initially curved (arches) clamped–clamped microbeams actuated by a dc load. The microbeams were fabricated by deep reactive ion etching technologies. They showed several results demonstrating the possibilities of snap-through or pull-in, depending on the level of curvature of the arch and the electrostatic load. Their simulations were based on the Galerkin method, and they have shown good agreement among their theoretical and experimental results.

Among the few works on the dynamics of curved microbeams, Krylov and Dick [17] studied the transient response of arches when actuated by suddenly applied step voltages. They showed several interesting phase portraits to illustrate the various scenarios of escape from one potential well of the arch to the other and also for the escape out of the global well through dynamic pull-in. Terré *et al.* [13] studied theoretically and experimentally the possibility of triggering the snap-through motion of a comb-drive actuated buckled microbeams driven dynamically at resonance. They have shown

Manuscript received July 19, 2009; revised February 23, 2010; accepted March 9, 2010. Date of publication April 29, 2010; date of current version June 3, 2010. This work was supported by the National Science Foundation (NSF) under Grant 0700683 and NSF CAREER Award 0846775. Subject Editor D. Elata.

M. I. Younis, H. M. Ouakad, R. Miles, and W. Cui are with the Department of Mechanical Engineering, Binghamton University–State University of New York, Binghamton, NY 13902 USA (e-mail: myounis@binghamton.edu; houakad1@binghamton.edu; miles@binghamton.edu; weilicui@yahoo.com).

F. M. Alsaleem was with the Department of Mechanical Engineering, Binghamton University–State University of New York, Binghamton, NY 13902 USA. He is now with Microstaq Inc., Austin, TX 78744-1052 USA (e-mail: falsale1@binghamton.edu).

Color versions of one or more of the figures in this paper are available online at http://ieeexplore.ieee.org.

Digital Object Identifier 10.1109/JMEMS.2010.2046624

that this snap-through motion can be used to realize a switch actuated at reduced voltage. Li *et al.* [19]–[21] investigated the nonlinear dynamics of initially buckled piezoelectrically driven microbeams. Static, free, and forced vibrations have been investigated. It was shown that a buckled microbeam can vibrate in a softening or hardening behavior, depending on the thickness of the microbeam. Buchaillot *et al.* [22] explored theoretically and experimentally the dynamic snap-through phenomenon of clamped–clamped buckled microbeams when subjected to base excitation and undergoing large vibration. Several scenarios of snap-through and chaotic-like behavior have been shown for a variety of excitation levels. Cabal and Ross [23] devised a methodology based on a mathematical model to describe theoretically the snap-through phenomena of a bilayer micromachined curved beam. Poon *et al.* [24] studied the dynamic response of a buckled clamped–clamped curved beam to sinusoidal excitation using a Runge–Kutta numerical integration method. Their work predicted various features, such as softening and hardening behaviors and chaotic motion of intermittent snap-through.

This paper is concerned with clamped–clamped micromachined arches, which are made curved intentionally through the induced residual stress from fabrication. By reviewing the state of the art, one can see that the dynamic behavior of clamped–clamped shallow arches under harmonic electrostatic forces has been rarely investigated. In previous works [25]–[30], we presented analytical and computational methods, and reduced-order models (ROMs) to investigate the static and dynamic behaviors of straight microbeams under electrostatic and electric harmonic loads. In this paper, we develop a ROM and utilize it to investigate the static and dynamic behaviors of clamped–clamped shallow arches when actuated by a dc load superimposed to an ac harmonic load. We explore the response of the arch for various loading ranges, which result in a variety of interesting nonlinear dynamics phenomena, including softening behaviors, dynamic snap-through, and dynamic pull-in. Our motivation of this investigation is that deep understanding of the dynamic behavior of these structures is needed to explore and enable their utilization and potential as sensors and actuators. We show preliminary results due to this dynamic actuation, which can be promising for MEMS filter and switch applications. We do not intend in this paper to study the switching dynamics or the post pull-in behavior. Such issues need a model that takes into account factors, such as the bouncing effect and the adhesion forces, which are beyond the scope of this paper.

The organization of this paper is as follows. Section II gives a short background on the two-well potential problem of a shallow arch and the dynamic snap-through and pull-in instabilities. In Section III, we present a model and derive a ROM of an electrically actuated clamped–clamped shallow arch. In Section IV, we study the static behavior of an arch under the actuation of a dc load. We select the arch parameters of [15] for the theoretical investigations of Sections IV and V to enable the demonstration of the snap-through phenomena without pull-in, which cannot be achieved using the fabricated beam of Section VI. In Section V, the dynamic response of the shallow arch when excited by a dc load superimposed to an ac harmonic load is simulated. Results are shown for several excitation frequencies near the fundamental natural frequency of the arch, its secondary resonances, and near its second and third natural frequencies. Section VI describes the experimental setup and the curved microbeam used for testing. In Section VII, the dynamics of the curved microbeam are investigated experimentally and compared with the theoretical results. Finally, we summarize the results and give some conclusions in Section VIII.

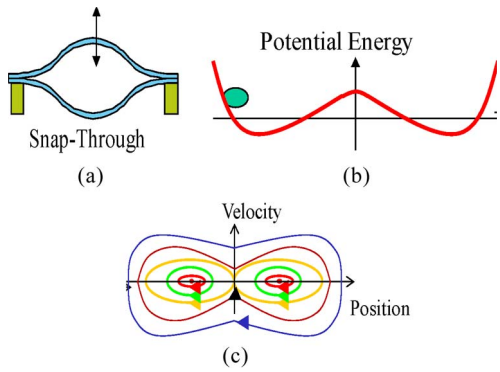

Fig. 1. (a) Shallow arch undergoing a snap-through motion. (b) Total potential energy of the arch. (c) Corresponding phase portrait.

II. Background

A. Dynamics of a Shallow Arch

A shallow arch can vibrate around its original deformed shape, around its opposing symmetric configuration, and in between those two shapes (snap-through motion) with large amplitude vibrations, Fig. 1(a). The potential energy of a shallow arch is of a double-well type, Fig. 1(b). With sufficient kinetic energy, a local vibration near one well can transfer to the other or escape to the global attractor in the case of snap-through motion, Fig. 1(c). The initial deformed configuration of the arch and its immovable edges results in strong influence of quadratic and cubic geometric nonlinearities on the structure behavior [31]. Because of its rich nonlinear phenomena, shallow arches and the problem of two-well potential have received special attention in the nonlinear dynamics literature [31], [32].

B. Dynamic Pull-In and Dynamic Snap-Through

Dynamic pull-in refers to the collapse of a movable electrode to a stationary electrode of a capacitor due to the combined action of its kinetic and potential energies. Sources of kinetic energy can be due to transient effects, for example due to a sudden step actuation of the microstructure or due to dynamic loading, for example, due to an ac harmonic voltage. Sources of potential energy are due to the elasticity or restoring forces of the microstructure and to the dc load actuation. Dynamic pull-in requires lower values of dc voltage to be triggered compared to the static pull-in threshold [30], [33]–[35].

Snap-through is another instability, which characterizes structures, such as buckled beams and arches. Similar to pull-in, snap-through can be triggered statically or dynamically. This can be also noted from Fig. 1, which indicates the possibility of snap-through due to the combined effect of kinetic and potential energies of the arch. Dynamic snap-through has been investigated thoroughly in the literature since the 1960s [36].

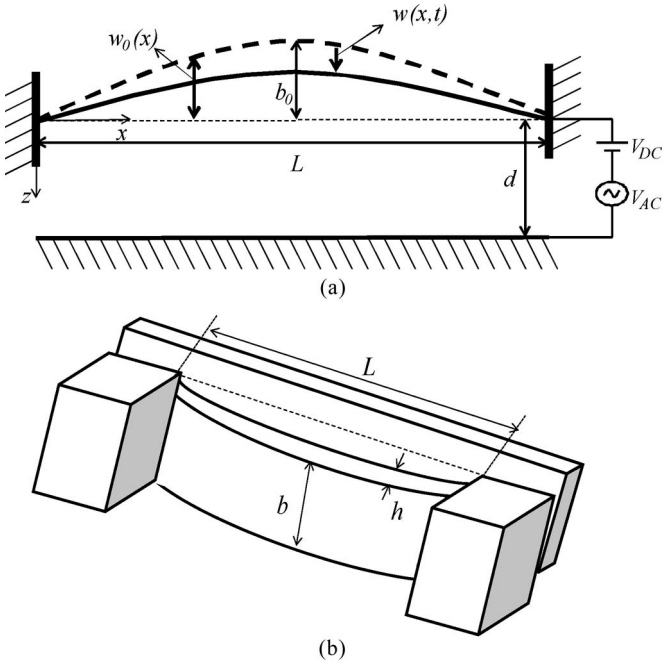

Fig. 2. (a) Schematic of the electrically actuated clamped–clamped arch. (b) 3-D schematic of the arch.

III. Problem Formulation

In this section, we formulate the problem governing the behavior of a MEMS shallow arch. Here, we consider a clamped–clamped shallow arch, Fig. 2, of initial shape $w_0(x) = -b_o[1 - \cos(2\pi x/L)]/2$, where b_0 is the initial rise, actuated by an electrode underneath it with a gap width d using a dc load superimposed to an ac harmonic load $V_{\rm AC}$ of frequency $\tilde{\Omega}$. Assuming a Euler–Bernoulli beam model, the nonlinear equation of motion governing the transverse deflection $w(x,t)$ of the arch of width b, thickness h, and length L is expressed as [14], [15], [31]

$$EI\frac{\partial^4 w}{\partial x^4} + \rho A\frac{\partial^2 w}{\partial t^2} + \tilde{c}\frac{\partial w}{\partial t} = \frac{\varepsilon b\left[V_{\rm DC} + V_{\rm AC}\cos(\tilde{\Omega}t)\right]^2}{2(d - w_o - w)^2} + \frac{EA}{2L}\left[\frac{\partial^2 w}{\partial x^2} + \frac{d^2 w_o}{dx^2}\right] \times \left[\int_0^L \left\{\left(\frac{\partial w}{\partial x}\right)^2 + 2\left(\frac{\partial w}{\partial x}\frac{dw_0}{dx}\right)\right\} dx\right] \quad (1)$$

where $E = 166$ GPa is the effective Young's modulus of the arch: $E = \hat{E}/(1-\nu^2)$, where $\hat{E} = 154$ GPa and $\nu = 0.27$ are the Young's modulus and Poisson's ratio of silicon, to account for the fact that the arch beam is wide [14], [15], $A = bh$ is the cross-sectional area, I is the moment of inertia, $\rho = 2332$ Kg/m^3 is the material density, and $\tilde{c}$ is the viscous damping coefficient.

The boundary conditions of the considered clamped–clamped arch are

$$w(0,t) = 0 \qquad \frac{\partial w}{\partial x}(0,t) = 0$$
$$w(L,t) = 0 \qquad \frac{\partial w}{\partial x}(L,t) = 0. \quad (2)$$

For convenience, we introduce the following nondimensional variables:

$$\hat{w} = \frac{w}{d} \qquad \hat{w}_0 = \frac{w_0}{d} \qquad \hat{x} = \frac{x}{L} \qquad \hat{t} = \frac{t}{T} \quad (3)$$

where T is a time constant defined by $T = \sqrt{\rho AL^4/EI}$. Next, we drop the hats for convenience. Therefore, the nondimensional equations of motion and associated boundary conditions can be written as

$$\frac{\partial^4 w}{\partial x^4} + \frac{\partial^2 w}{\partial t^2} + c\frac{\partial w}{\partial t} = \alpha_2\frac{\left[V_{\rm DC} + V_{\rm AC}\cos(\Omega t)\right]^2}{(1 - w_o - w)^2} + \alpha_1\left[\frac{\partial^2 w}{\partial x^2} + \frac{d^2 w_o}{dx^2}\right] \times \left[\int_0^1 \left\{\left(\frac{\partial w}{\partial x}\right)^2 + 2\left(\frac{\partial w}{\partial x}\frac{dw_0}{dx}\right)\right\} dx\right] \quad (4)$$

$$w(0,t) = 0 \qquad \frac{\partial w}{\partial x}(0,t) = 0$$
$$w(1,t) = 0 \qquad \frac{\partial w}{\partial x}(1,t) = 0 \quad (5)$$

where

$$\alpha_1 = 6\left(\frac{d}{h}\right)^2 \qquad \alpha_2 = \frac{\varepsilon bL^4}{2EId^3} \qquad \Omega = \frac{\tilde{\Omega}}{\omega_n}$$
$$c = \frac{\tilde{c}L^4}{EIT} \qquad w_0(x) = -\frac{b_0}{2d}\left[1 - \cos(2\pi x)\right] \quad (6)$$

and $\omega_n = 1/T$.

One can see that the last term of (4) contains quadratic and cubic nonlinearities. When the arch is actuated by a dc load, its equilibrium position changes. This gives rise to additional quadratic nonlinearity terms. The interaction among all these nonlinearities can play a crucial role in the response of the arch. To simulate the response of the arch, (4) and (5) are discretized using the Galerkin procedure to yield a ROM [27], [28]. Hence, the deflection of the arch is approximated as

$$w(x,t) = \sum_{i=1}^{n} u_i(t)\phi_i(x) \quad (7)$$

where $\phi_i(x)(i = 1, 2, \ldots, n)$ denotes the normalized linear undamped mode shapes of the straight microbeam $(w_0 = 0)$, and $u_i(t)(i = 1, 2, \ldots, n)$ denotes the nondimensional modal coordinates. To obtain the ROM, we first multiply (4) by $F(x,t) = (1 - w_0 - w)^2$. This reduces the computational cost since the electrostatic force term in the discretized equation will not require complicated numerical integration (integrating a numerator term over a denominator term numerically is computationally expensive) [27], [28]. Then, substituting (7) into the resulting equation, multiplying by $\phi_i(x)$, and then

integrating the outcome from zero to one yield the following differential equations in terms of the modal coordinates $u_i(t)$:

$$\sum_{i=1}^{n} \ddot{u}_i \int_0^1 \{\phi_i(x)\phi_j(x)F(x,t)\,dx\} + c\sum_{i=1}^{n} u_i(t) \int_0^1 \{\phi_i(x)\phi_j(x)F(x,t)\,dx\} + \sum_{i=1}^{n} u_i(t) \int_0^1 \{\phi_i^{iv}(x)\phi_j(x)F(x,t)\,dx\} = \alpha_2 \left[V_{\mathrm{DC}} + V_{\mathrm{AC}}\cos(\Omega t)\right]^2 \int_0^1 \phi_j(x)\,dx + \alpha_1 \int_0^1 \left(\sum_{i=1}^{n} u_i(t)\phi_i'(x)\right)^2 dx \times \int_0^1 \{\phi_j(x)F(x,t)G(x,t)\}\,dx - 2\alpha_1 \int_0^1 \left(\sum_{i=1}^{n} u_i(t)\phi_i'(x)\frac{dw_0}{dx}\right) dx \times \int_0^1 \{\phi_j(x)F(x,t)G(x,t)\}\,dx, \quad j = 1,\ldots,n \tag{8}$$

where

$$G(x,t) = \sum_{i=1}^{n} u_i(t)\phi_i''(x) + \frac{d^2 w_0}{dx^2}. \tag{9}$$

To simulate the dynamic behavior, (8) is integrated with time. To simulate the static response, all time-dependent terms in (8) are set equal to zero, and then, the modal coordinates $u_i(t)$ are replaced by unknown constant coefficients $a_i (i = 1, 2, \ldots, n)$. This results in a system of nonlinear algebraic equations in terms of the coefficients a_i. The system is then solved numerically using the Newton–Raphson method to obtain the static deflection of the arch.

IV. Static Response

As a case study, we consider the silicon clamped–clamped shallow arch of Krylov *et al.* [15] of $L = 1000$ μm, $h = 2.4$ μm, $b = 30$ μm, $d = 10.1$ μm, and initial rise $b_o = 3.5$ μm. First, we examined the contribution from the antisymmetric modes in the ROM and found it negligible for the static analysis (unlike the case cited in [37] for a deep arch loaded by a static point load). Next, we examine the convergence of the ROM. Fig. 3 shows the maximum static deflection of the shallow arch (midpoint deflection) when using one up to six symmetric mode

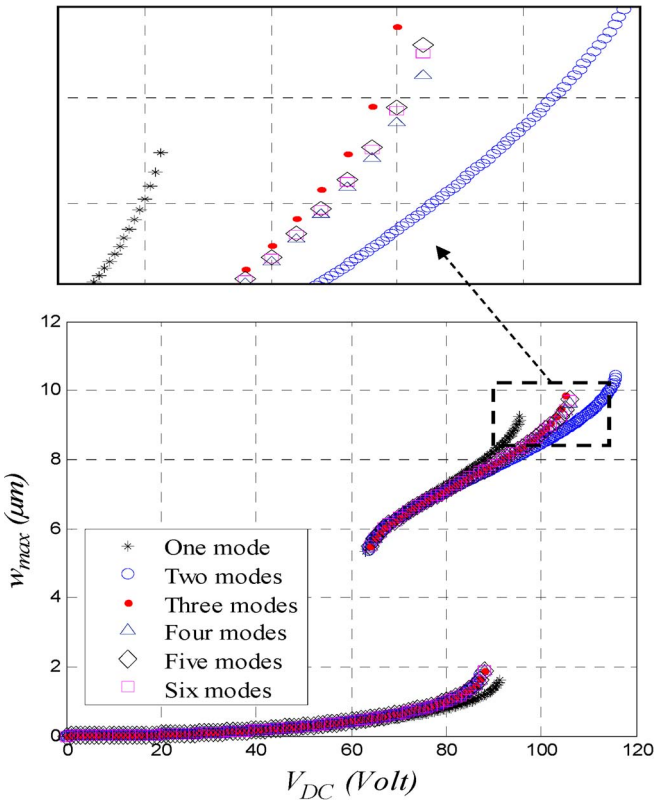

Fig. 3. Variation of the static deflection of the shallow arch with the dc voltage for various numbers of mode shapes of a straight beam in the ROM.

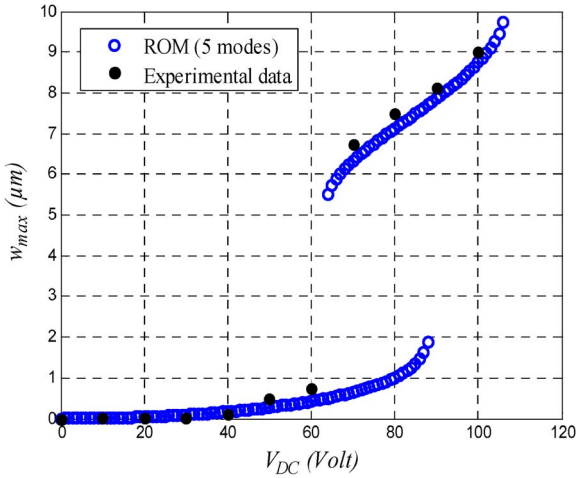

Fig. 4. Comparison between the obtained static deflection of the shallow arch with the dc voltage using five-mode shapes in the ROM with the experimental data of Krylov *et al.* [15].

shapes of a straight clamped–clamped beam in the ROM while varying the dc load. It follows from the figure that using five symmetric modes yields acceptable converged results. As can be seen in the figure, the shallow arch undergoes a snap-through motion near $V_{\mathrm{DC}} = 88$ V and, then, a pull-in instability near $V_{\mathrm{DC}} = 106$ V.

In Fig. 4, we validate the five-mode ROM results for the clamped–clamped arch by comparing them with the experimental data reported in [15]. It is clear that the experimental data and the ROM results are in good agreement except near

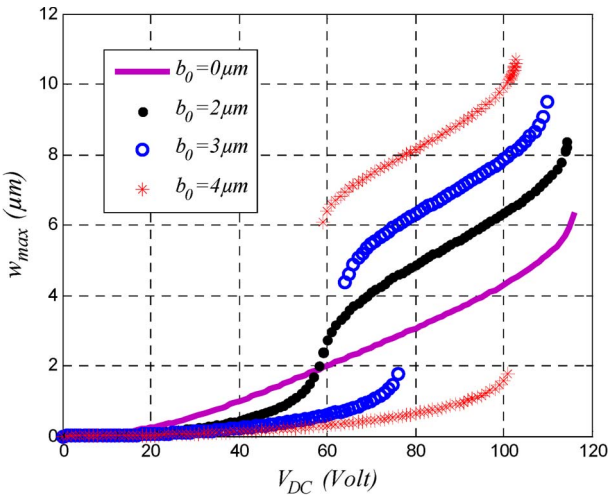

Fig. 5. Variation of the static deflection of the shallow arch with the dc voltage for various values of initial rise b_0.

snap-through and pull-in. Similar deviation has been observed by Krylov *et al.* [15], which they have attributed to the inertia and dynamic effect in the experiment, which are not being modeled in the static analysis. According to Zhang *et al.* [14], this discrepancy can be attributed to several factors, including the possible inhomogeneity of the beam, the stress experienced by the beam ends that is larger than the other parts of the beam, the dynamic effect, and the possibility of the presence of unwanted moments at the beam ends due to the coupling between the force acting on the beam ends and friction.

In Fig. 5, the effect of the initial rise on the static deflection of the arch is shown. For $b_o = 2$ μm, the arch behaves more like a beam with no discontinuity in its deflection as $V_{\rm DC}$ increases. For the cases of $b_o = 3$ μm and $b_o = 4$ μm, the arch snaps through first and then pulls in while increasing $V_{\rm DC}$. Moreover, the figure shows that the values of dc voltage, where the arch snaps through, increase with b_o, while the pull-in voltage decreases with increasing b_o. This indicates that the stiffness of the shallow arch increases before snap-through and then decreases in the buckled position with the increase of b_o. Increasing b_o further results in direct pull-in without the intermediate snap-through jump. These behaviors were also reported in [14] and [15].

V. Response to DC and AC Harmonic Loads

In this section, we study the dynamic behavior of the shallow arch due to a combined dc and ac harmonic loads near the primary and secondary resonances. We should mention here that the actuation of the arch with a dc load alone may shift its natural frequencies to lower values. In addition, varying the curvature level can affect the natural frequencies. More details on this can be found in [38] and [39]. We integrate the differential equations in terms of the modal coordinates numerically with time using the Runge–Kutta technique to simulate the dynamic response. Here, we use both symmetric and antisymmetric mode shapes in the ROM to capture any possible crossing among the resonances of the symmetric and antisymmetric modes.

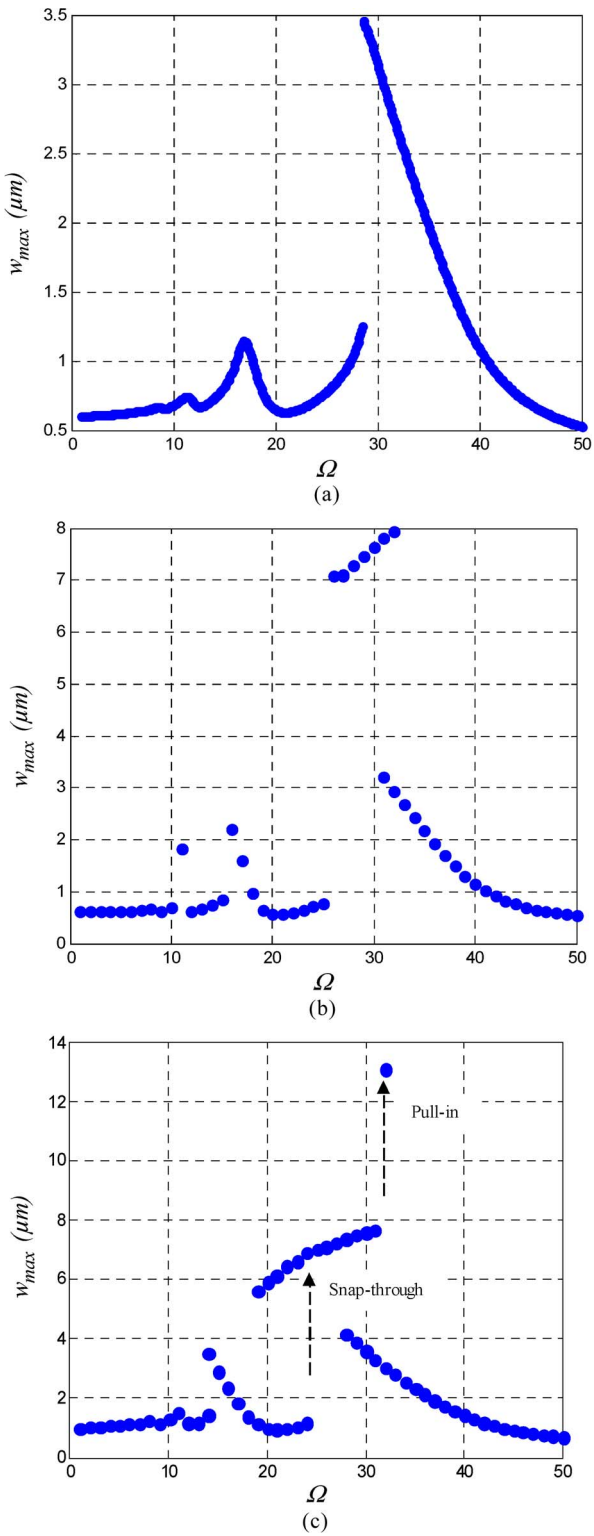

Fig. 6. Simulated frequency-response curves of a shallow arch actuated by dc and ac harmonic loads, showing several scenarios of nonlinear behaviors for an initial rise $b_0 = 3$ μm. (a) $V_{\rm DC} = 40$ V, $V_{\rm AC} = 20$ V, and $\zeta = 0.1$. (b) $V_{\rm DC} = 40$ V, $V_{\rm AC} = 20$ V, and $\zeta = 0.005$. (c) $V_{\rm DC} = 40$ V, $V_{\rm AC} = 40$ V, and $\zeta = 0.1$.

In Fig. 6(a)–(c), we simulate the dynamic response of the arch investigated in Section IV with an initial rise of $b_o = 3$ μm to various values of dc and ac loads and damping ratios. These values have been selected to demonstrate various nonlinear behaviors of the arch. A damping ratio ζ is assumed, which

is related to the viscous damping coefficient c as $c = 2\zeta\omega$, where ω is the nondimensional natural frequency. Fig. 6(a) shows the response for $V_{\rm DC} = 40$ V, $V_{\rm AC} = 20$ V, and $\zeta = 0.1$. Three distinctive resonances are observed, which are primary resonance near the fundamental natural frequency and another two secondary resonances. These are superharmonic resonances of order one-half (near $\Omega = 17$) and one-third (near $\Omega = 12$), which indicate the presence of both quadratic and cubic nonlinearities. Note that the quadratic nonlinearities are due to both the electrostatic forces and the curvature of the arch [the terms multiplying α_1 and involving w_0 in (4)], whereas the cubic nonlinearity is due to mid-plane stretching, as indicated in the term multiplying α_1 that does not involve w_0 in (4).

It is clear from the figure that the quadratic nonlinearity is dominant over the cubic one since the superharmonic resonance of order one-half is of larger amplitude than that of order one-third and also since all resonances exhibit softening behavior (the frequency-response curves bend to the left). Fig. 6(a) shows that the softening behavior appears before the snap-through motion, where the vibration occurs around the local attractor of one of the potential wells of the arch.

Fig. 6(b) shows the dynamic response of the arch when the damping ratio is reduced to $\zeta = 0.005$, which should lead to larger overall response. The figure shows the secondary resonances with the softening behavior but with larger amplitude compared to Fig. 6(a). Near the primary resonance, the response seems of softening type except near a narrow band of frequency, in which the response jumps to larger values where it exhibits a hardening behavior. In this narrow band, the arch snaps through and jumps from the local attractor to a bigger global attractor. Hence, it vibrates in large amplitude motion across the two wells [see the big blue orbit in Fig. 1(a)], where the hardening effect of the cubic nonlinearity becomes dominant. A similar observation has been reported for the vibration of buckled beams [24]. One possible use of this sudden jump of response in a narrow frequency range in MEMS is a bandpass filter [40]. The instantaneous jump in the response to the snap-through regime means a sharp roll-off from the stopbands to passband, which is a desirable property of filters. Of course, the possibility of hysteresis and the stability of the snap-through vibration are some of the dynamical issues that need to be further investigated for this idea.

Fig. 6(c) shows the response of the arch when the ac amplitude is raised to $V_{\rm AC} = 40$ V while keeping the other parameters as in Fig. 6(a). This case is an example of very large excitation. Near the primary resonance, one can see a large band of snap-through motion with clear hardening behavior. Moreover, the snap-through amplitude continues to increase with the increase of excitation frequency until the motion is terminated by dynamic pull-in. This series of interesting jumps can be of great potential for designing MEMS switches and actuators of large strokes and low-power consumptions. This is because dynamic actuation demands less voltage for pull-in compared to static methods [13], [29], [30]. For example, one can excite the arch such that it escapes from the local well of small vibrations to pull in directly without the intermediate snap-through oscillation. This case will be demonstrated theoretically and experimentally in the next section.

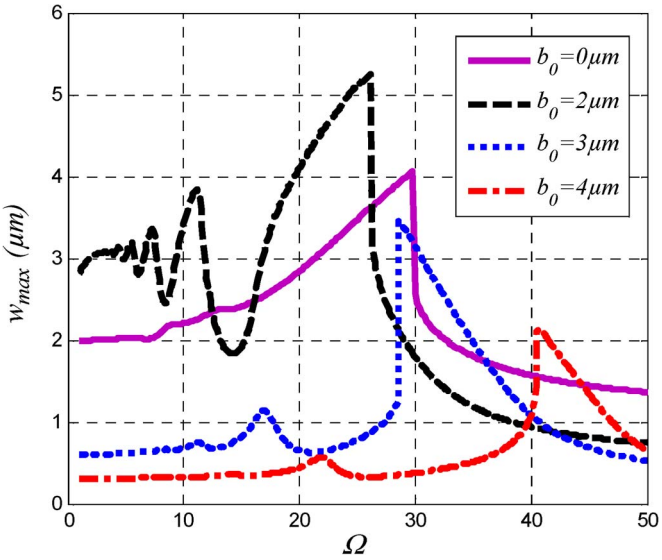

Fig. 7. Simulated frequency-response curves of a shallow arch actuated by dc and ac harmonic loads for $V_{\rm DC} = 40$ V, $V_{\rm AC} = 20$ V, $\zeta = 0.1$, and various values of initial rise b_0.

Next, we show in Fig. 7 the effect of the initial rise on the dynamic response of the arch. Results are also shown for $b_o = 0$, which is the case of a straight clamped–clamped microbeam to enable comparison with arches. Note here that all the frequency-response curves start at $w_{\rm max}$, corresponding to the equilibrium position at $V_{\rm DC} = 60$ V shown in Fig. 5 (quasi-static behavior at slow excitation frequency). First, one can see that there is an increase in the linear natural frequency of the arch with increasing b_o, as expected based on the conclusion of Fig. 5 that increasing b_o strengthens the stiffness of the arch, with the exception of the case of $b_o = 2$ μm. This is because, at $V_{\rm DC} = 60$ V, the curved beam in this case shows a snap-through-like behavior, as shown in Fig. 5. For $b_o = 3$ μm and $b_o = 4$ μm, the frequency-response curve shows a softening-type behavior. This indicates that the softening effects and the quadratic nonlinearities of the electrostatic force and the curvature are dominant. The cases of the straight microbeam and the "almost-curved" beam $b_o = 2$ μm show a hardening-type behavior. In this case, the cubic mid-plane stretching effect dominates the other quadratic nonlinearities.

In electrostatically actuated systems, secondary resonances can appear in their responses due to the strong influence of the nonlinear electrostatic force, which is quadratic in nature. These resonances can have significant influence on the performance of the systems. Fig. 8 shows the arch dynamics near the subharmonic resonance of order one-half (excitation near twice the fundamental natural frequency) for two values of $V_{\rm AC}$. The damping ratio in this figure is taken to be $\zeta = 0.005$ to enable the activation of the subharmonic resonance [29], [34]. It turns out in this case that this range of frequency is also close to the second natural frequency of the arch. Hence, one can see that the subharmonic resonance curves cross those of the second natural frequency resonances. Such an interesting phenomenon may trigger internal resonances between the first and second modes of the arch [31].

We end up this section by showing results for exciting the arch near its third natural frequency, Fig. 9. The figure shows

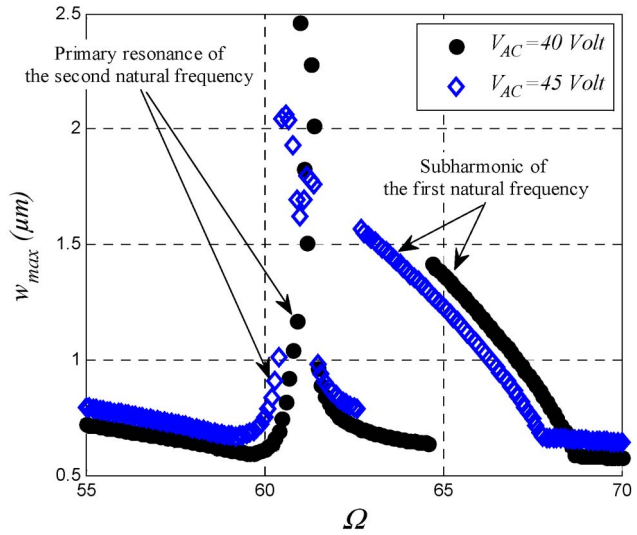

Fig. 8. Simulated frequency-response curves near the subharmonic resonance of order one-half, which turns out to be also close to the second natural frequency of the arch. In the figure, $V_{\rm DC} = 40$ V, $\zeta = 0.005$, and $b_0 = 3$ μm.

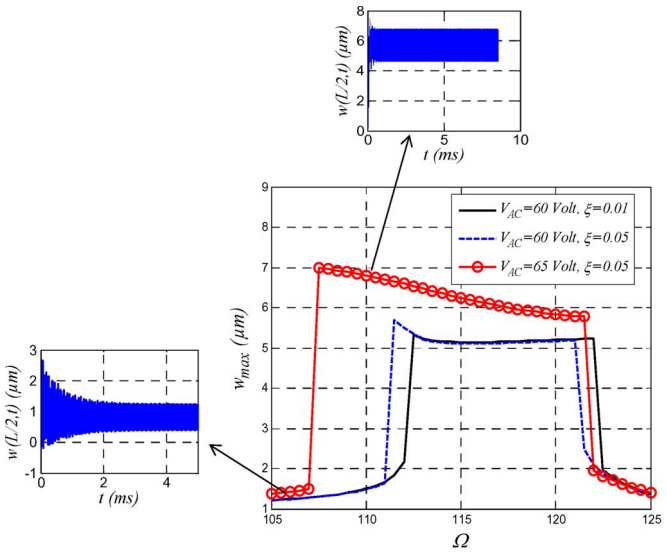

Fig. 9. Simulated frequency-response curves of a shallow arch excited near its third mode for various ac loads and damping ratios and for $V_{\rm DC} = 60$ V and $b_0 = 3.5$ μm.

that the arch oscillates in small amplitude around one of its stable state before passing resonance. Then, it jumps to the other symmetric well to vibrate in small motion around the other stable state for a wide range of frequencies, after which it returns back and jumps to its original potential well. This sort of behavior could be also promising to build a bandpass filter with a sharp roll-off from the stopbands to passband, a flat bandwidth, and a high center frequency [40]. Fig. 9 shows also that $V_{\rm AC}$ and damping ratio can be used to control the bandwidth and the center frequency of such a filter.

VI. Experimental Setup

The experimental work of this paper was conducted on a silicon chip containing curved polysilicon microbeams. The curvature of the microbeams was realized by residual stresses during fabrication. These are induced because of the difference in thermal expansion coefficients of the deposited beam layers and the substrate. The microbeams were fabricated using surface micromachining process at the Cornell Nano-Scale Facility. Fig. 10 shows the fabrication process flow of the polysilicon curved microbeams. The microbeam fabrication starts with the growth of a layer of sacrificial wet oxide on a bare silicon wafer, followed by the deposition of a polysilicon layer as the microbeam material [Fig. 10(a)]. The thickness of the oxide layer was measured to be $\sim$0.8 μm ($\pm$ μm). It acts as an etch stop in the next step for the polysilicon etch that defines the microbeams and contact pads [Fig. 10(b)] and holds the microbeams in place firmly until the final release. The thickness of the polysilicon was measured with a P10 profilometer to be $\sim$1.3 μm ($\pm$0.1 μm). The wafer is then diced into microbeam chips. The microbeams are fully released at the chip level by dissolving the sacrificial oxide layer in hydrofluoric acid [Fig. 10(c)]. A very thin layer of chrome/gold (approximately 50 Å/50 Å) is evaporated on the microbeams to enhance the electrical conductivity [Fig. 10(d)].

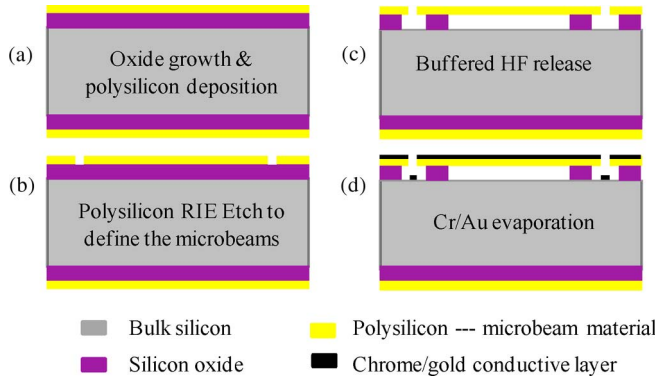

Fig. 10. Fabrication process flow of the polysilicon microbeams.

The microbeams were wire bonded to a printed circuit board, Fig. 11(a). A curved microbeam of length 300 μm and width 50 μm is chosen for this investigation. Fig. 11(b) shows a 3-D image of the surface profile of the microbeam, as measured using a Wyko profilometer. It was found that the beam is initially curved up with an initial rise of approximately 1 μm. Moreover, the Wyko measurement revealed a total thickness of the microbeam with the gap underneath near 2.2 μm. Fig. 11(c) shows the experimental setup used for testing the dynamics of the curved microbeam and monitoring its motion. The setup includes an MSA motion analyzer, which is a high-frequency laser Doppler vibrometer, and a vacuum chamber equipped with ports for electrical connections, pressure gauge, and a viewport window made of a quartz glass that enables the laser to penetrate without any distortion.

VII. Experimental Data and Comparison With Simulations

This section presents a comparison between the experimental data and the ROM results for the dynamic response of the curved polysilicon microbeam described in Section VI. For the theoretical model, we estimated $d = 0.85$ μm and $h = 1.35$ μm based on the Wyko measurements in Section VI.

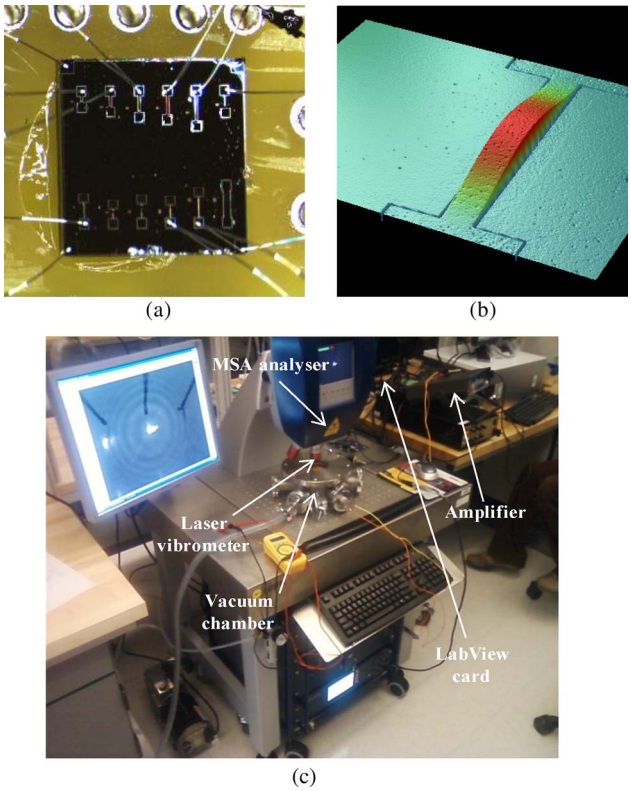

Fig. 11. (a) Chip of polysilicon curved clamped–clamped microbeams wire-bonded to a printed circuit board. (b) 3-D Vecco profiler image for the tested curved microbeam. (c) Experimental setup used for testing the curved microbeam.

The frequency responses of the curved beam during a forward-sweep frequency test for different ac voltages are shown in Fig. 12. The figure shows that, for all the ac voltages, the frequency-response curves undergo a softening behavior similar to the predictions in Section V. Because the fabricated arch has a very small gap, separating it from the substrate, it was not possible to obtain experimentally a snap-through motion without pull-in. Instead, we were able to detect the jump from the stable operation near the local well of the arch to pull in directly. Fig. 13(a) shows an experimental result of this case. Increasing the ac load further creates a pull-in zone, Fig. 13(b), where the microbeam is forced to pull in if operated within this zone of frequency [34]. This figure was obtained using both forward and backward frequency sweep tests. Comparing the simulation results with the experimental data in Figs. 12 and 13 shows good agreement, thereby validating the theoretical results.

VIII. Conclusion and Summary

The static response of an arch due to a dc load actuation has been simulated, and the results were validated by comparing them to experimental data. The dynamic behavior of an electrically actuated clamped–clamped shallow arch has been investigated theoretically and experimentally. The arch is actuated by a dc load superimposed to an ac harmonic load. The results show various scenarios of static and dynamic snap-through and pull-in, depending on the initial rise of the arch and the electrostatic load level. Furthermore, our investigation also

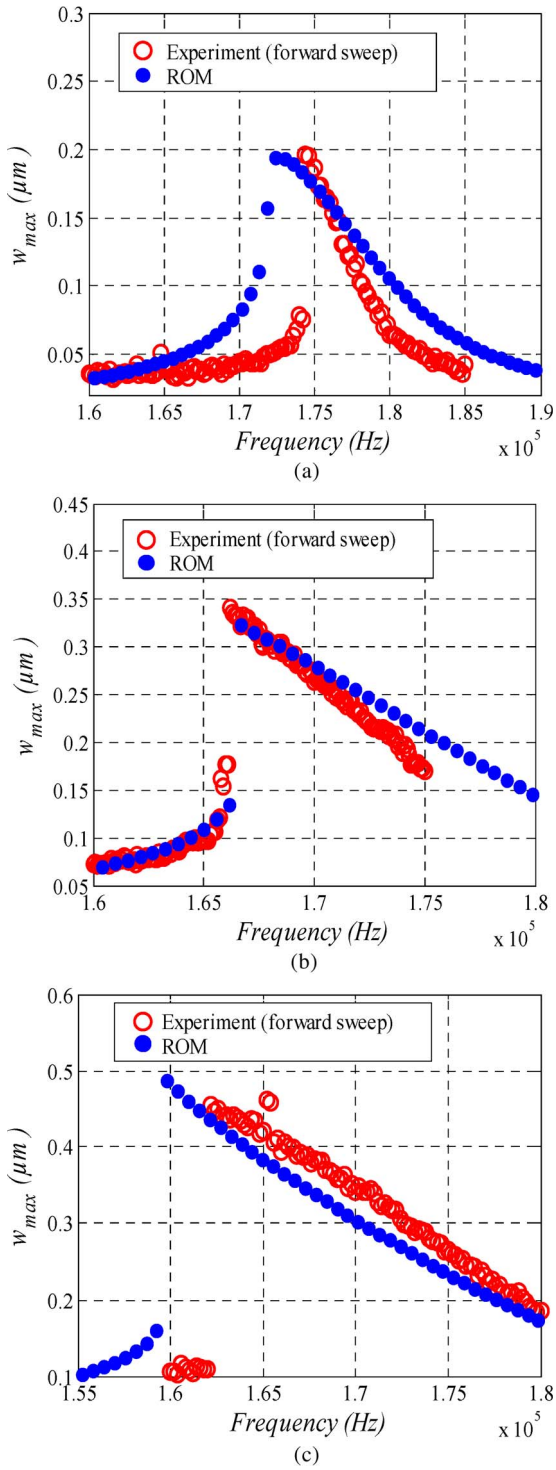

Fig. 12. Experimental data versus simulation results using a five-mode ROM for the frequency-response of the fabricated arch for $V_{DC} = 5$ V and various ac loads and pressure values inside the vacuum chamber. (a) $V_{AC} = 2.4$ V; pressure = 120 mtorr ($\zeta = 0.025$). (b) $V_{AC} = 4.5$ V; pressure = 124 mtorr ($\zeta = 0.035$). (c) $V_{AC} = 7.1$ V; pressure = 145 mtorr ($\zeta = 0.04$).

predicts that the initial rise of the shallow arch has a significant effect on reducing its hardening behavior and increasing its softening behavior. Simulation results were shown demonstrating various scenarios of resonances, including primary and subharmonic resonances. Moreover, resonances near higher order harmonics were presented. Promising results were shown

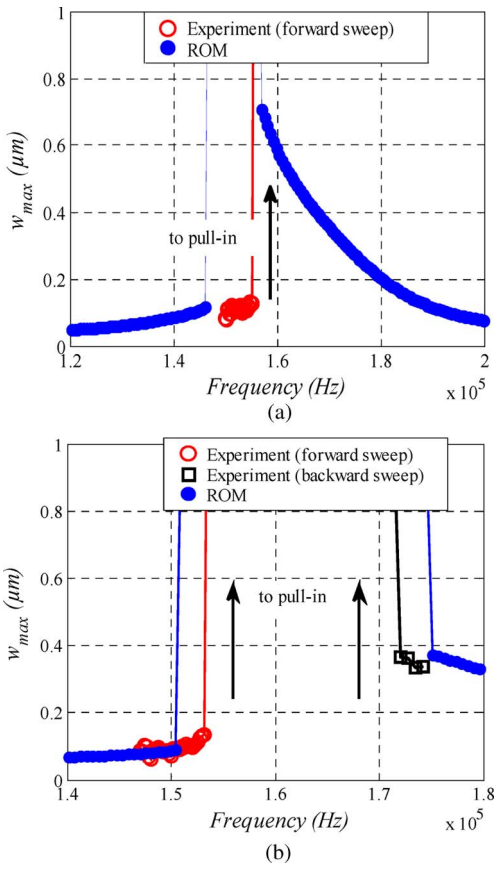

Fig. 13. Experimental data versus simulation results, showing dynamic pull-in and pull-in band when $V_{\rm DC}=5$ V. (a) $V_{\rm AC}=9.4$ V; pressure $=120$ mtorr ($\zeta=0.025$). (b) $V_{\rm AC}=14$ V; pressure $=115$ mtorr ($\zeta=0.02$).

for the possibility of using the dynamic snap-through motion of the arch near specific bands of frequencies to realize bandpass filters of sharp transition from the passband to stopbands and also of flat bandwidth. In addition, a bandpass filter of higher center frequency was demonstrated by exciting the arch near its third mode. More research needs to be conducted to investigate the feasibility of using this system as a filter. Experimental work has been conducted to test arches made of polysilicon curved microbeams to dynamic ac and dc actuation. The experimental results were shown to be in good agreement with the simulations.

Future research is planned to analyze, in more details, the rule of the various nonlinearities of the electrostatically actuated arch. Moreover, future work is planned to confirm many of the presented theoretical results based on the shooting technique for finding periodic motions [29], [30], [34].

REFERENCES

[1] J. Qui, J. H. Lang, and A. H. A. Slocum, "Curved-beam bistable mechanism," *J. Microelectromech. Syst.*, vol. 13, no. 2, pp. 137–146, Apr. 2004.
[2] J. S. Go, Y. Cho, B. M. Kwak, and P. Kwanhum, "Snapping microswitch with adjustable acceleration threshold," *Sens. Actuators A, Phys.*, vol. 54, no. 1–3, pp. 579–583, Jun. 1996.
[3] J. Rossiter, B. Stoimenov, and T. Mukai, "A self-switching bistable artificial muscle actuator," in *Proc. SICE-ICASE Int. Joint Conf.*, Busan, Korea, Oct. 2006, pp. 18–21.
[4] R. A. M. Receveur, C. R. Marxer, R. Woering, V. C. M. H. Larik, and N. F. de Rooij, "Laterally moving bistable MEMS DC switch for biomedical applications," *J. Microelectromech. Syst.*, vol. 14, no. 5, pp. 89–98, Oct. 2005.
[5] B. Charlot, W. Sun, K. Yamashita, H. Fujita, and H. Toshiyoshi, "Bistable nanowire for micromechanical memory," *J. Micromech. Microeng.*, vol. 18, no. 4, p. 045 005, Feb. 2008, 1088/0960-1317.
[6] J. S. Han, J. S. Ko, Y. T. Kim, and B. M. Kwak, "Parametric study and optimization of a micro-optical switch with a laterally driven electromagnetic microactuator," *J. Micromech. Microeng.*, vol. 12, no. 6, pp. 39–47, Oct. 2002.
[7] J. S. Ko, M. G. Lee, J. S. Han, J. S. Go, B. Shin, and D.-S. Lee, "A laterally-driven bistable electromagnetic microrelay," *ETRI J.*, vol. 28, no. 3, pp. 389–392, 2006.
[8] S. Park and D. Hah, "Pre-shaped buckled-beam actuators: Theory and experiment," *Sens. Actuators A, Phys.*, vol. 148, no. 1, pp. 186–192, Nov. 2008.
[9] A. Michael and C. Y. Kwok, "Design criteria for bi-stable behavior in a buckled multi-layered MEMS bridge," *J. Micromech. Microeng.*, vol. 16, no. 10, pp. 34–43, Aug. 2006.
[10] J. Qui, J. H. Lang, A. H. Slocum, and A. C. Weber, "A bulk-micromachined bistable relay with U-shaped thermal actuators," *J. Microelectromech. Syst.*, vol. 14, no. 5, pp. 99–109, Oct. 2005.
[11] M. T. A. Saif, "On a tunable bistable MEMS-theory and experiment," *J. Microelectromech. Syst.*, vol. 9, no. 2, pp. 157–170, Jun. 2000.
[12] M. Sulfridge, T. Saif, N. Miller, and M. Meinhart, "Nonlinear dynamic study of a bistable MEMS: Model and experiment," *J. Microelectromech. Syst.*, vol. 13, no. 5, pp. 725–731, Oct. 2004.
[13] J. C. Terre, A. F. Marques, and A. M. Shkel, "Snap-action bistable micromechanics actuated by nonlinear resonance," *J. Microelectromech. Syst.*, vol. 17, no. 5, pp. 1082–1093, Oct. 2008.
[14] Y. Zhang, Y. Wang, Z. Li, Y. Huang, and D. Li, "Snap-through and pull-in instabilities of an arch-shaped beam under an electrostatic loading," *J. Microelectromech. Syst.*, vol. 16, no. 3, pp. 684–693, Jun. 2007.
[15] S. Krylov, B. R. Ilic, D. Schreiber, S. Seretensky, and H. Craighead, "The pull-in behavior of electrostatically actuated bistable microstructures," *J. Micromech. Microeng.*, vol. 18, no. 5, pp. 055 026-1–055 026-20, Apr. 2008.
[16] S. Krylov and S. Seretensky, "Pull-in and multistability analysis of an initially curved beam," presented at the Asia-Pacific Conf. Transducers Micro-Nano Technology, Singapore, Jun. 25–28, 2006, Paper D-27.
[17] S. Krylov and N. Dick, "Pull-in dynamics of electrostatically actuated bistable micro beam," presented at the ASME Int. Design Engineering Technical Conf. Computers Information Engineering Conf., San Diego, CA, Aug. 30–Sep. 2, 2009, Paper DETC2009-87236.
[18] K. Das and R. C. Batra, "Pull-in and snap-through instabilities in transient deformations of microelectromechanical systems," *J. Micromech. Microeng.*, vol. 19, no. 3, pp. 035 008-1–035 008-19, Feb. 2009.
[19] H. Li and B. Balachandran, "Buckling and free oscillations of composite microresonators," *J. Microelectromech. Syst.*, vol. 15, no. 1, pp. 42–51, Feb. 2006.
[20] H. Li, S. Preidikman, B. Balachandran, and C. D. Mote, Jr, "Nonlinear free and forced oscillations of piezoelectric microresonators," *J. Micromech. Microeng.*, vol. 16, no. 2, pp. 356–367, Jan. 2006.
[21] H. Li, S. Preidikman, D. J. DeVoe, and B. Balachandran, "Nonlinear oscillation of piezoelectric microresonators with curved cross-section," *Sens. Actuators A, Phys.*, vol. 144, no. 1, pp. 194–200, May 2008.
[22] L. Buchaillot, O. Millet, E. Quévy, and D. Collard, "Post-buckling dynamic behavior of self-assembled 3D microstructures," *Microsyst. Technol.*, vol. 14, no. 1, pp. 69–78, Jan. 2007.
[23] A. Cabal and D. S. Ross, "Snap-through bilayer microbeam," in *Proc. Tech. Int. Conf. Model. Simul. Microsyst. (Nanotech)*, 2002, vol. 1, pp. 230–233.
[24] W. Y. Poon, C. F. Ng, and Y. Y. Lee, "Dynamic stability of a curved beam under sinusoidal loading," *Proc. Inst. Mech. Eng., J. Aerosp. Eng.*, vol. 216, no. 4, pp. 209–217, 2002.
[25] E. M. Abdel-Rahman, M. I. Younis, and A. H. Nayfeh, "Characterization of the mechanical behavior of an electrically actuated microbeam," *J. Micromech. Microeng.*, vol. 12, no. 6, pp. 766–795, Sep. 2002.
[26] M. I. Younis and A. H. Nayfeh, "A study of the nonlinear response of a resonant microbeam to an electric actuation," *Nonlinear Dyn.*, vol. 31, no. 1, pp. 91–117, Jan. 2003.
[27] H. M. Nayfeh, M. I. Younis, and E. M. Abdel-Rahman, "Reduced-order models for MEMS applications," *Nonlinear Dyn.*, vol. 41, no. 1–3, pp. 211–236, Aug. 2005.
[28] M. I. Younis, E. M. Abdel-Rahman, and A. H. Nayfeh, "A reduced-order model for electrically actuated microbeam-based MEMS," *J. Microelectromech. Syst.*, vol. 12, no. 5, pp. 672–680, Oct. 2003.

[29] A. H. Nayfeh and M. I. Younis, "Dynamics of MEMS resonators under superharmonic and subharmonic excitations," *J. Micromech. Microeng.*, vol. 15, no. 10, pp. 1840–1847, Aug. 2005.
[30] A. H. Nayfeh, M. I. Younis, and E. M. Abdel-Rahman, "Dynamic pull-in phenomenon in MEMS resonators," *Nonlinear Dyn.*, vol. 48, no. 1/2, pp. 153–163, Apr. 2007.
[31] A. H. Nayfeh, *Nonlinear Interactions*. New York: Wiley-Interscience, 2000.
[32] F. C. Moon, *Chaotic Vibrations: An Introduction for Applied Scientists and Engineers*. Hoboken, NJ: Wiley-Interscience, 2004.
[33] S. Krylov and R. Maimon, "Pull-in dynamics of an elastic beam actuated by continuously distributed electrostatic force," *J. Vib. Acoust.*, vol. 126, no. 3, pp. 332–342, Jul. 2004.
[34] F. M. Alsaleem, M. I. Younis, and H. M. Ouakad, "On the nonlinear resonances and dynamic pull-in of electrostatically actuated resonators," *J. Micromech. Microeng.*, vol. 19, no. 4, pp. 045 013-1–045 013-14, Mar. 2009.
[35] D. Elata and H. Bamberger, "On the dynamic pull-in of electrostatic actuators with multiple degrees of freedom and multiple voltage sources," *J. Microelectromech. Syst.*, vol. 15, no. 1, pp. 131–140, Feb. 2006.
[36] J. Humphreys, "On dynamic snap buckling of shallow arches," *AIAA J.*, vol. 4, no. 5, pp. 878–886, May 1966.
[37] A. B. Pippard, "The elastic arch and its modes of instability," *Eur. J. Phys.*, vol. 11, no. 6, pp. 359–365, Nov. 1990.
[38] M. I. Younis and H. M. Ouakad, "The static and dynamic behavior of MEMS arches under electrostatic actuation," in *Proc. 6th IEEE-ISMA*, Sharjah, United Arab Emirates, Mar. 2009, pp. 1–6. DOI: 10.1109/ISMA.2009.5164821.
[39] H. M. Ouakad, M. I. Younis, F. M. Alsaleem, R. Miles, and W. Cui, "The static and dynamic behavior of MEMS arches under electrostatic actuation," presented at the ASME Int. Design Engineering Technical Conf. Computers Information Engineering Conference, San Diego, CA, Aug./Sep. 2009. Paper DETC2009-87024.
[40] V. M. Varadan, K. J. Vinoy, and K. A. Jose, *RF MEMS and Their Applications*. New York: Wiley, 2003.

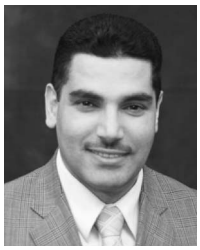

Mohammad I. Younis received the B.S. degree in mechanical engineering from Jordan University of Science and Technology, Irbid, Jordan, in 1999, and the M.S. and Ph.D. degrees in engineering mechanics from Virginia Polytechnic Institute and State University, Blacksburg, in 2001 and 2004, respectively.

Since 2004, he has been an Assistant Professor in the Department of Mechanical Engineering, Binghamton University–State University of New York, Binghamton, where he is currently the Director of the MEMS Motion and Characterization Laboratory. He serves as an Associate Editor for *Mathematical Problems in Engineering*. He is the holder of a U.S. patent for a MEMS switch triggered by acceleration and shock and has another pending one on MEMS mass and gas detectors. His research interests are in the area of nonlinear dynamics and vibration of MEMS and NEMS with applications for sensing and actuation.

Dr. Younis was a recipient of a 2009 National Science Foundation CAREER Award. He is a member of the American Society of Mechanical Engineers.

Hassen M. Ouakad received the B.S. degree in mechanical engineering from the Tunisia Polytechnic School (Ecole Polytechnique de Tunisie), La Marsa, Tunisia, in 2007, and the M.S. degree in computational mechanics from the Tunisia Polytechnic School in 2008 in collaboration with the Department of Engineering Science and Mechanics, Virginia Polytechnic Institute and State University, Blacksburg. His M.S. thesis included work on the design, analysis, and control of MEMS actuators and sensors. He is currently working toward the Ph.D. degree in the Department of Mechanical Engineering, Binghamton University–State University of New York, Binghamton, NY.

His research is focused on the modeling and simulation of the nonlinear structural mechanics of MEMS/NEMS.

Dr. Ouakad is a Student Member of the American Society of Mechanical Engineers.

Fadi M. Alsaleem received the B.S. degree in mechatronics engineering from Hashemite University, Zarqa, Jordan, in 2003, a graduate certificate in mechatronics engineering from the American University of Sharjah, Sharjah, United Arab Emirates, and the M.S. and Ph.D. degrees in mechanical engineering from Binghamton University–State University of New York, Binghamton, in 2007 and 2009, respectively. His Ph.D. research was focused on utilizing the nonlinear dynamic response of MEMS devices to device new mass and acceleration sensors.

Since 2009, he has been a MEMS Control Engineer at Microstaq Inc., Austin, TX, where he is controlling novel MEMS fluidic valves in heating, ventilating, and air conditioning systems to enhance their energy efficiency.

Dr. Alsaleem is a Student Member of the American Society of Mechanical Engineers.

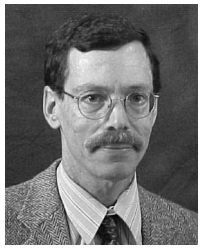

Ronald Miles received the B.S.E.E. degree from the University of California (UC), Berkeley, in 1976, and the M.S. and Ph.D. degrees in mechanical engineering from the University of Washington, Seattle.

In 1977, he began work on structural acoustics and noise control at Boeing that lasted for eight years. He was an Assistant Research Engineer and a Lecturer in the Department of Mechanical Engineering, University of California at Berkeley. Since 1989, he has been with the Department of Mechanical Engineering, Binghamton University–State University of New York, Binghamton, where he has served as the Director of Graduate Studies, the Director of Undergraduate Studies, an Associate Chair, a Department Chair, and a Professor, and is currently an Associate Dean for Research in the Watson School of Engineering and Applied Science. He has published over 80 scholarly articles and presented over 70 invited lectures. His primary research is on the development of biologically inspired microacoustic sensors.

Dr. Miles is the recipient of the University Award for Excellence in Teaching; the Chancellor's Award for Excellence in Teaching; the Research Foundation's Outstanding Inventor Award; the Chancellor's Award for Research in Science, Engineering and Medicine; the Research Foundation's Innovation, Creation and Discovery Award; and the Research Foundation's 2005 First Patent Award. He is a member of the American Society of Mechanical Engineers.

Weili Cui received the B.S.M.E. degree from Southwest Jiaotong University, Chengdu, China, and the Ph.D. degree in mechanical engineering from Binghamton University–State University of New York, Binghamton, in 2004.

Prior to earning his doctoral degree, he was employed for three years as a Manufacturing Process Engineer at the Beijing Feb. 7th Locomotive Factory, Beijing, China. While at Binghamton, he developed his core specialization: the analysis, design, and fabrication of biologically inspired MEMS silicon microphones. Since earning his Ph.D. in 2004, he has continued this work and is currently the Team Leader of an externally funded fabrication group at SUNY, where he conducts the work at the Cornell NanoScale Science and Technology Facility. He has also developed interdisciplinary collaborations with other researchers in the areas of modeling and fabrication of microfluidic channels, carbon nanotubes, and microbeams. He currently has one U.S. patent application pending and 21 publications.

Dr. Cui is a member of the American Society of Mechanical Engineers.